Efficient Deep Learning Approach for Detection of Brain Tumor Disease

https://doi.org/10.3991/ijoe.v19i06.40277

Syefy Mohammed Mangj(✉), Payman Hussein Hussan,
Wafaa Mohammed Ridha Shakir
Babylon Technical Institute, Al-Furat Al-Awsat Technical University, Kufa, Iraq
inb.syffi10@atu.edu.iq

Abstract—This article presents, we describe fully autonomous brain tumor classifying as well as the classification method depending on a multiscale DCNN Deep-Convolutional-Neural-Network (multiscale Deep Convolutional Neural Network). As compared to similar efforts, ours differs in part because it processes input images at two different spatial scales using independent neural networks. The suggested neural model can interpret MRI scans comprising two kinds of tumors: the first one meningioma, and the second one glioma, without requiring input images to be preprocessed to eliminate skull and spine components. The effectiveness we've noted model available to the public MRI image dataset containing 3060 slices of 250 cases is compared to previously reported models for conventional ML (machine learning) as well as DL (deep learning). In the comparison, our approach produced an impressive 97% accuracy in classifying tumors, which was better than some other algorithms utilizing similar datasets.

Keywords—classifying of brain tumor, DL, CNN, multiscale process, ML, MRI

1 Introduction

The segmentation and classifying of medical pictures serve a crucial role in brain tumor diagnosis, growth prediction, and treatment. Patients with brain tumors have a better chance of surviving if their condition is diagnosed and treated quickly. Brain tumor detection and categorization in large medical image databases, performed manually for regular clinical tasks, are labor- and time-intensive. A process for automatic detection, localization, and classification is required and worth the effort [1]. Many medical imaging techniques are utilized to collect diagnostic information regarding tumors (tumor kind, size, form, position, and others) [2]. The most effective methods are (CT, SPECT, PET, MRS, and MRI). It is possible to combine these methods to gain more specific information on tumors. Nonetheless, MRI is the most popular technology due to its positive qualities. In MRI image acquisition, the scan produces hundreds of two-dimensional picture slices with great soft tissue opposition and without the use of ionizing irradiance [2]. There are 4 MRI diagnostic modes: (T1 or T2 weight MRI),

(T1-CE), as well as (FLAIR MRI) exist all kinds of magnetic resonance imaging. Each MRI modality provides tissue-distinct pictures, making some better than others for searching specific tissues. T1 is often utilized for working with healthy tissues. T2 pictures are better suitable for recognizing edema region borders. Although FLAIR images help diagnose an edematous CSF area, T1-CE images show tumor margins [3]. The purpose of MRI image analysis is to recognize and classify brain cancers, our work demonstrates that the T1-CE modality was competent as well as sufficient. BTI has grown significantly during the past few decades. In recent years, quantitative magnetic resonance imaging (MRI) investigations of brain malignancies have proliferated [2, 4]. The BTS method is used in biopsies to identify tumor-infected tissue from normal tissue. The segmentation problem is transformed into a classification challenge [5] due to the widespread usage of pixel categorization in BTS applications for the purpose of isolating brain tumors in images. The purpose of this study is to develop and assess a DL method for MCNN-based brain tumor classification and segmentation. The proposed neural network [6] was trained and validated using a T1-CE Input image dataset of 250 cases that included meningiomas and gliomas. Illustrations of these two kinds of tumors are depicted in Figure 1A and B. In additional info on a dataset is provided.

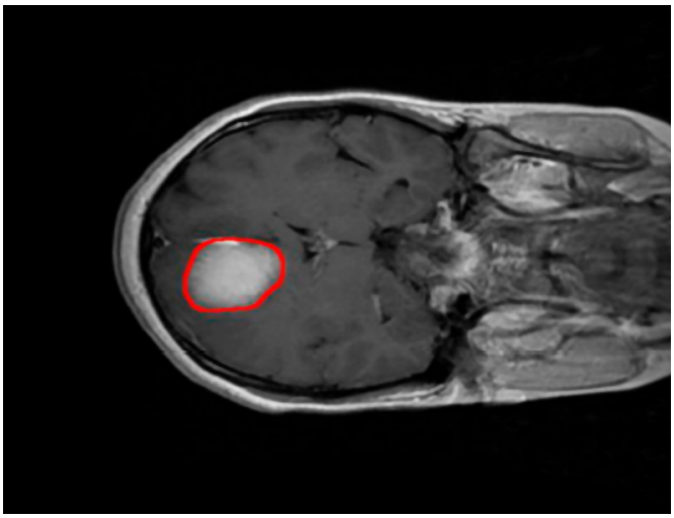

Fig. 1A. Red highlights the tumor borders in T1-CE MRI scans of a meningioma

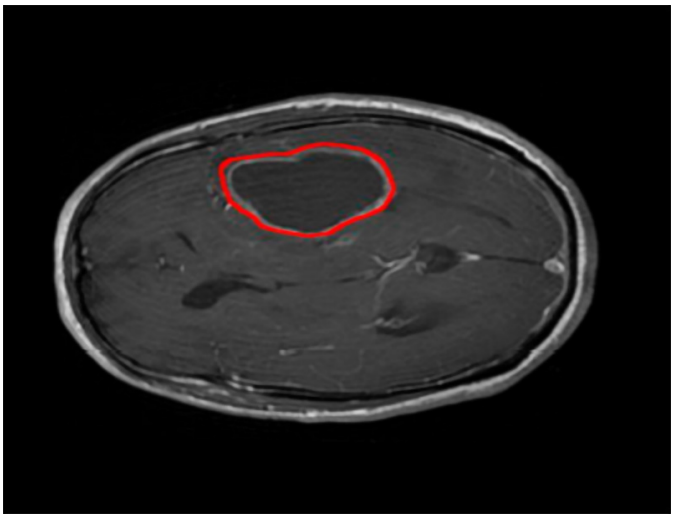

Fig. 1B. Red highlights the tumor borders in T1-CE MRI scans of a Glioma

Both generative and discriminative approaches to tumor segmentation may be found widely used in the BTS sector. Discriminative approaches, on the other hand, use the best practice expert segmentation method to learn image features and their connections [2], and piece generative methods use explicit anatomic modeling to obtain the segmentation. Discriminative research published in the past has tended to use conventional ML [7–10] but has recently shifted to adopting DL approaches [11–15].

2 Related work

In works that employ traditional ML approaches, The segmentation pipeline has a feature extraction preprocessing stage. Despite its flaws, skull stripping is a common preprocessing step in traditional discriminative methods, which includes parameter selection, the need for prior picture knowledge, and a long computing time [7, 16, 17]. The collected characteristics act as input to the classifying and/or segmentation phase. Moreover, the study [7, 18], presented SVM and ANN algorithm classifiers were compared, the accuracy was between 79% and 91% for SVM, between 75% and 94% for ANN, using 10 characteristics as well as a Back Propagation Network classifier (BPNC). In [8], suggested an automatic tumor classification system with an accuracy of 95%. In addition [9] fractal wavelet features were supplied to a SOM classifier for 90% precision. The KNN classifier is used in a semi-automatic fashion in instance-based training tumor identification pipelines [10]. Using well-known BRATS-2013 data, they reported Dice similarities of 85% and 75% between the entire tumor and its core, placing them in the second location among full plus core tests. As ML approaches have progressed, they've moved on to the next stage, which is training computers to determine which features are most indicative of a dataset. This approach is the core of DNN [5], which transforms feature-driven issues in data-driven challenges. CNN [19], as well as

FCN [20, 21], have been used in an assortment of tasks within DNN. DL's introduction has had a significant effect on the development of medical imaging equipment, which is why it is put to use in both general image analysis [22] as well as medical image analysis [1, 5, 23, 24] as researchers have widely implemented improved techniques in recent years [25]. The advancements in the field have made collaboration between ML scientists with radiologists quite interesting [26]. In [11], the authors investigated the application of an FCN algorithm again for BRATS-2013 dataset, after that the KNN classifier suggestion [10] was discussed. The majority of current research utilizing DL to classify brain tumors dataset [27] is focused on CNNs or FCNs. In [12], brain tissue, including white matter hyperintensities were segmented using an MCNN. They measured the accuracy of their CNN architecture using data from the MRBrainS13 competition [13]. The most significant contributions to the field were made by [14], who presented an innovative CNN program titled U-net. They employed this CNN model to segregate brain areas from ISBI challenge electron microscopy images [15]. U-net consists of five convolutional stages and five D-convolutional stages, forming a U, hence its name. They achieved the highest scores in the ISBI competition [15].

3 Methodology

3.1 Substances and approaches

Suggested CNN and execution specifics. For tumor segmentation, we suggest a multi-path CNN model, as depicted in Figure 2. Using a PX-by-PX approach, the CNN model analyses an MRI image (slice) and assigns each PX to one of three possibility action output labels: label zero depiction (area of healthy), label one depiction (tumor of meningioma), label two depiction (tumor of glioma).

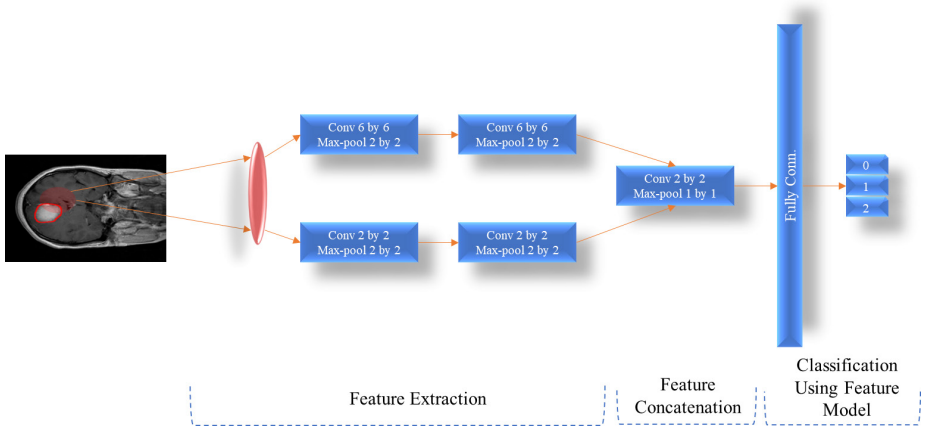

Fig. 2. The suggested CNN model

Our model uses sliding windows. So, each PX classifies based on N by N neighborhood or window, which our CNN model uses as input (as shown in the previous Figure). Each window is transformed through two convolutional routes using large-scale, medium-scale, and small-scale kernels get featured. Our window sizes were 10 by 10, 6 by 6, and 2 by 2 pixels. After preliminary configuration and testing with 32 by 32 PX and 74 by 74 PX windows, the window size was chosen. Each path has two convolutional phases with ReLU rectification and a 2-by-2 maximum-pooling kernel with stride 1. The path for the big-scale, medium-scale and small-scale each have 95 and 63 feature maps, respectively. The scale features from the 2nd path are combined with a convolutional layer using a 2x2 ReLU activation function kernel and a 1x1 maximum pooling kernel with a stride of 1. This phase output enters the FC phase, where 8,281 scale features are concatenated to provide the classification method. Before the FC layer, our model adds the dropout layer to prevent overfitting. The last layer's activation function is soft max. The suggested CNN has been executed by utilizing PyTorch. Around 3M trainable parameters exist in the NN (2,845,921). The tests were run on a Linux Foundation cloud infrastructure powered by a Core i7 processor. The average time to anticipate an image was 60 seconds after 6 days of training.

Datasets and preprocess. CE-MRI of the brain is typically only available in two dimensions and with a consi erable slice gap in clinical settings. Thus, the proposed method employs one-dimensional slices from 250 examples, such as meningiomas (706 slices) and gliomas (3060 slices) (1,415 slices). Figure 1 depicts many forms of tumors. This dataset is composed of four K-fold cross-validation indices. As a result, 70% (2441) of images are utilized for training, whereas 30% (612 images) serve the purpose of assessing progress, then five times repeat. The in-plane resolution of the images is 512 by 512 PX, or 0.48 by 0.48 meters. The slices are 1 meter apart and 6 mm thick. Two skilled radiologists manually sketch the tumour borders. Every dataset slice is associated with the patient's pid. During training, elastic transform data augmentation [27] inhibits neural network overfitting. Figure 3 depicts this change. Data augmentation increases the number of training images to 4904 per fold iteration. A thorough technique collected 6 px 6 every image inside the training dataset used as a training example, which included 150 TP and 325 TN window occurrences per tumor. Pixel normalization scaled these window PX throughout the training dataset (null mean and units' variance).

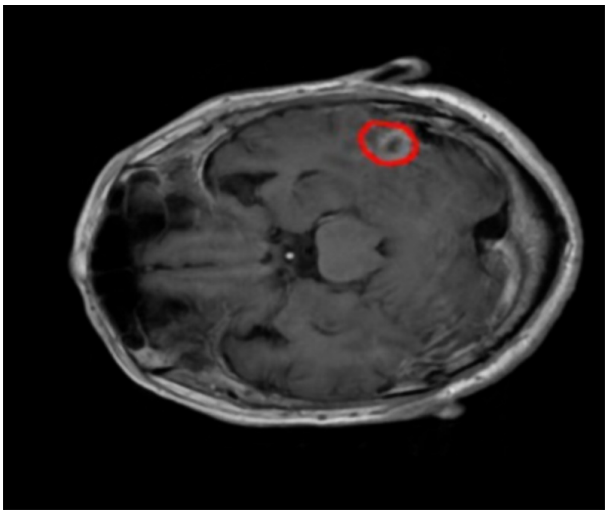

(A)

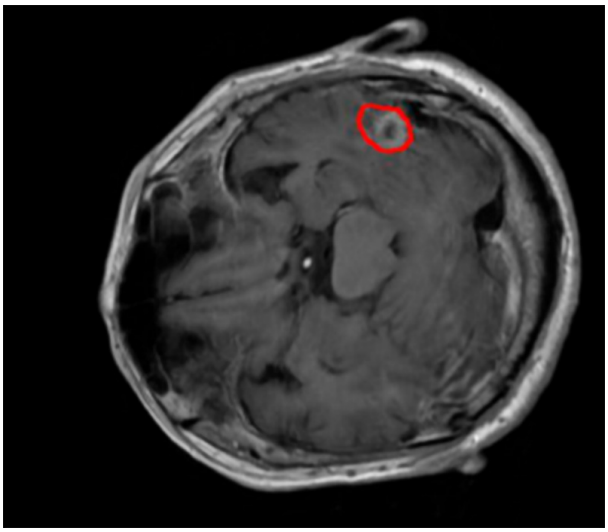

(B)

Fig. 3A and B. Data augmentation by elastic transformation, tumor borders have been accented with red color

3.2 Training neural networks and execution measures effectiveness

Using the slice train/test subsets from the dataset, the recommended CNN and performance metrics were obtained using a 4-fold cross-validation approach, as previously stated. To train the suggested model, for this, we employed the SGD algorithm with initial values of 0.004 for the learning rate and 0.8 for the velocity coefficient, and ran the training for 70 epochs for each fold iteration. We also used a rate-of-change of the learning rate, exponentially decreasing every 10 epochs. The dropout parameter was set to a value of 0.4.

There were 612 images used to verify the model's accuracy inside each fold using a sliding window technique. Each testing window was 6 PX by 6 PX and was fed into the trained CNN to predict the tumor type label, l p. To segment the tumor, the area containing all the PX for a certain tumor type is analyzed. Frames from the testing window are normalized before being fed into the CNN using the global average and standard deviation of PX in the train windows, both of which were computed during data preparation. The classification function can be computed by labeling each PX (i,j) in the input slice (Eq. 1 and 2). The vector is used in a classification function. $\{f_1, l = 1,2\}$ to determine the label l_p, which indicates the tumor type in a particular slice. The classification function establishes a link between the label prediction and the actual label, l, $\{P_{ij} = = l\}$ (amount of PX labeled including l) and the entirety of the prediction, $P_{ij} > 0$ (amount of PX including a predicted label that fit in to every tumor). The label of predicted, l_p will be associated with a connection label that is significantly bigger than the minimum relation required by the confidence criterion.

$$P_{ij}, \begin{cases} P_{ij}, = 0, & if\,(i,j)\,is\,healthy\,position \\ P_{ij}, = 1, & if\,(i,j)\,is\,meningioma\,tumor \\ P_{ij}, = 2, & if\,(i,j)\,is\,glioma\,tumor \end{cases} \tag{1}$$

$$f_1 = \begin{cases} \left| \frac{P_{ij} == 1}{P_{ij} > 0} \right| > \tau_c \\ 0 \end{cases} \tag{2}$$

$$l_p = \begin{cases} argmax\{f_1 > 0\} & if\,\{f_1 > 0\} \neq \{\varnothing\} \\ -1 & nonclassified \end{cases} \tag{3}$$

In this case, the size, or pixel number, is represented by the symbol |.| (amount of PX). We quantify effectiveness by calculating the Confusion Matrix, Dice score, and Sensitivity score [3]. In addition, we developed a score based on the ratio of expected tumor types, pattas, to assess a reliability of the anticipated tumor type. This index measures how large the tumor area $P_{ij} = lgt$ is in comparison to the total tumor area estimated by our approach $P_{ij} > 0$. The pattas index measures the ratio relative to the full predicted tumor, while the Sensitivity index measures it related to the actual tumor size. Assessment metrics are derived from the following Eqs:

$$Dice = \frac{2|P_1 \cap T_1|}{(|P_1| + |T_1|)} = \frac{2TP}{(2TP + FP + FN)} \tag{4}$$

$$Sensitivity(P,T) = \frac{TP}{(TP + FN)} \tag{5}$$

$$pattas = \frac{|P_1|}{|P > 0|} \tag{6}$$

where P_T is the amount of TP and FP is the amount of FP, FN is the amount of FN, ^ is the logical AND operation, |.| is the size or PX amount, P_1 act. The adding of TP and FP (the predicted positives (P), $P_{ij} = lgt$, and T1 act the adding of TP and FN $T_{ij} = 1$.

4 Outcomes and analysis

The NN was evaluated using the dataset's required 4-fold validation train/test subsets. The findings are presented in the tables and figures below. Figure 4A and B displayed the outcomes of our method applied to two distinct slices.

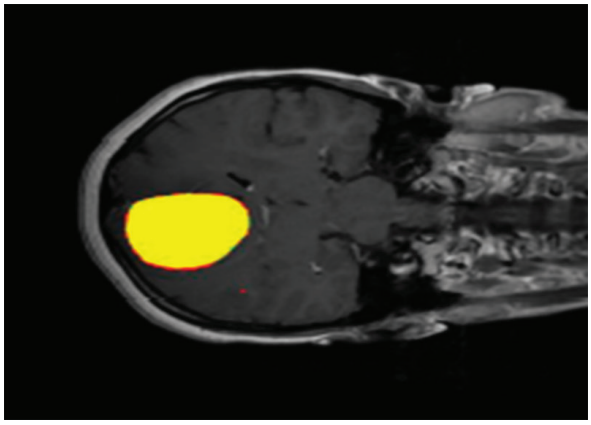

(A)

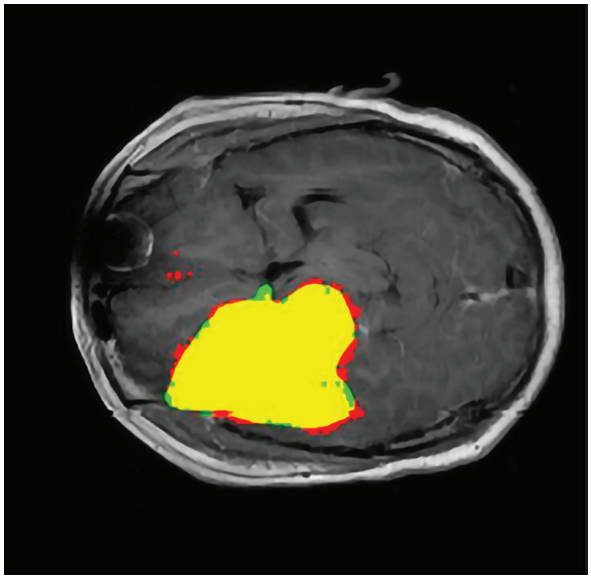

(B)

Fig. 4A and B. The outcomes of the suggested model for 2 slices (A) meningioma tumor, and (B) glioma tumor.

Obtaining segmentation metrics is displayed in Table 1. Meningioma photos had the highest Dice index and glioma images. Hence, glioma prediction has the highest FP, and FN percentage and meningioma prediction has the lowest. The TP-to-reality ratio was the weakest for glioma predictions. In contrast, Figure 4B shows a glioma has the highest pttas index and, Figure 4A shows a meningioma has the lowest pttas index. The segmentation metrics used to rank the 2 tumors all produced distinct results, which can be attributed to the unique characteristics of the brain tumors under study and the inclusion of additional variables. With average values for the segmentation, metrics are Dice = 82%, Sensitivity = 94%, and pattas = 96%, the segmentation metrics that were collected show remarkable results.

Table 1. Metrics for segmenting 3060 slices analyzed using 4-fold cross validation

Metricn/Tumor	Meningioma	Glioma	Avg
DICE	89%	77%	82%
SENSITIVITY	96%	90%	94%
PTTAS	93%	98%	96%

The histograms for these segmentation measures for each processed slice are displayed in Figure 5. The values of the histograms for Sensitivity and pttas are extraordinarily concentrated in a narrow region slightly below the maximum region. This indicates that the majority of processed images fare well across these criteria.

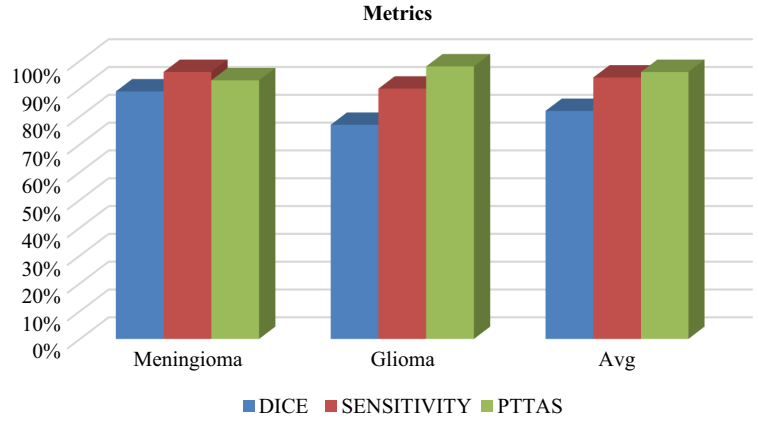

Fig. 5. Distributions of the metrics that were calculated after the data was analyzed

Figure 5 shows several examples surrounding 0. Pattas below 0.3 in these samples indicate a false tumor. (pattas measures right label ratio). Pattas over 0.3 indicate reliable tumor type prediction. All remaining samples had values above 0.4, suggesting accurate prediction. The high Sensitivity index indicates that almost all tumor area in processed images was correctly retrieved (area in yellow in Figure 4A and B). Dice histogram amplitude indicates FP and FN. The Dice index is high; hence FP and FN are quite low.

While, Figure 6A–D displays segmentations with mislabeled portions; in Figure 6A and B, the most of the diagnosed tumor is accurately tagged (red area), yielding in an extremely precise segmentation (yellow area). Regrettably, the spot discovered outside the brain was misidentified as a glioma tumor (green area). This example highlights how the inclusion of non-cerebral areas that can produce FP has enhanced the complexity of this dataset. This complexity is also evident in Figure 6C and D example. Similarly, the segmentation is accurate for the most part (yellow region), Nevertheless, In the area of the sphenoidal sinuses, wherein pituitary tumors commonly develop, there is a misclassified area designated as a pituitary tumor (blue area).

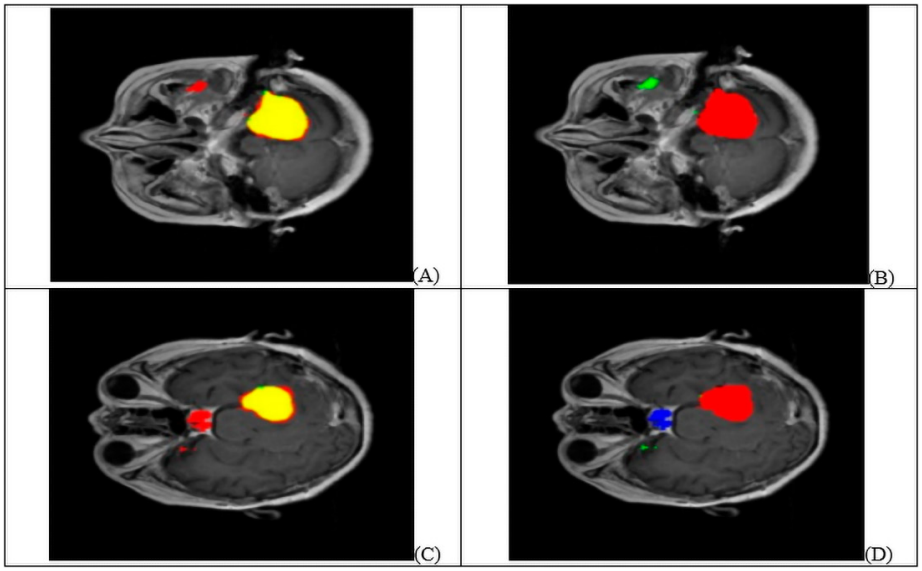

Fig. 6. Some sample outcomes from the suggested strategy for two slices representing meningioma and glioma

Due to the manner in which we segment the tumors, we can simply classify them. If the total number of projected tumor types for all pixels in the image exceeds the confidence threshold tc, the image's classification algorithm will classify that pixel as having the most probable form of tumor (Eq. 2). Tables 2 and 3 exhibit, confusion matrix values as well as tumor accuracy rate for the [6] method and our model. As evidenced by the high values in the diagonal of the confusion matrix, our method classifies tumors with a high degree of accuracy (97%).

Table 2. Predicted tumor confusion matrix [6], accuracy = 91%

Predict (T)	Meningioma Tumor	Glioma Tumor	Sensitiveness
Meningioma Tumor	570	58	86%
Glioma Tumor	43	1327	96%
Pituitary Tumor	76	53	87%
ACC = 91%			

Table 3. Predicted tumor confusion matrix for our method, taking a confidence threshold tc = 75%, and accuracy = 97%

Predict (T)	Tumor Meningioma	Tumor Glioma	Sensitiveness	Not Classified
Meningioma Tumor	659	4	93%	42
Glioma Tumor	7	1414	99%	4
Pituitary Tumor	1	3	98%	15
ACC = 97%				

5 Comparing with other studies

Our method's segmentation performance metrics (Table 1) are comparable to those of the winning solutions in the renowned BRATS brain tumor image segmentation competition, this criterion uses glioma tumor images from a dataset that includes four different MRI modalities (T1, T2, T1-CE, as well as FLAIR). Segmentation of the entire tumor yielded glioma Dice index values ranging from 82% to 96%. Despite the disadvantages of using a single MRI modality and differentiating between two types of tumors, our technique for glioma segmentation achieves a Dice index value of 77%, which is close to the greatest value achievable. Using the same T1-CE MRI image collection as prior studies would allow for a more relevant comparison of outcomes. The accuracy of our tumor classification system is compared in Table 4 to seven existing approaches, two of which are feature-driven [6, 28] and five of which are deep learning [6, 29, 30]. Our technique exceeds the competition with its 97% tumor classifying accurateness.

Table 4. Using the same dataset of T1-CE MRI images, the new approach is compared against existing ones

References	Classifying	ACC
[6]	SVM	91%
[28]	Fisher kernel	94%
[31]	CNN and GA	94%
Proposed method	MCNN	97%

The two experiments in [6, 28] are examples of traditional ML algorithms employing predefined feature extraction. In [6], Two independent methods were used to gather local characteristics from the expanded tumor site, and from these, a classification model was built: histogram of intensity, GLCM, and BoW. With the K-NN, these traits were used to generate a dictionary. The ROIs were then classified as a specific type of tumor using a trained classifier. SVM, SRC, and KNN classification techniques were compared. Utilizing BoW as wella ss SVM as a classifier yielded the best results. It was suggested in [28] to use a Fisher kernel for content-based image retrieval of MRI images. These approaches [6, 28] are semi-automatic because they begin with

segmentations conducted by expert radiologists. These require human interaction during categorization, whereas the solution we offer is totally automatic. With a 75% confidence criterion, our technique achieves a tumor classification accuracy of 97%, compared to 91% in [6] and 94% in [28]. In addition, Meningioma has the lowest Sensitivity score (Table 3) in the [6] method because the intensity difference between tumor and healthy areas is the smallest of all tumor types (Table 2). The sensitivity to gliomas is the greatest. Meningiomas and gliomas fall halfway between pituitary tumors. Lastly, in [27], a CNN was also proposed, but a genetic algorithm was We used these factors to determine the best settings for a convolutional neural network (CNN): the number of convolutional layers, the amount of maximum-pooling layers, the amount of fully-connected layers, its input vector, the dropout value, the optimization strategy, and the learning rate. Rotation, translation, scaling, and mirroring were employed to enrich the data. They achieved a 94% accuracy rate.

6 Conclusion

We presented a method for fully automatic tumor of brain segmentation as well as classification utilizing CNN model trained for multiscale processing. The effectiveness of the suggested strategy was determined by analyzing publicly available T1-weighted contrast-enhanced MRI data. Elastic transformation data augmentation was employed to prevent overfitting and expand scale of data used for training. Using the same dataset, we compared our findings to those of three different brain tumor classification algorithms. Our technique was found to have a 97% classification success rate for cancers. To segment and classify meningioma and glioma, we employ a multiscale CNN technique that exploits two distinct processing routes. Despite the fact that portions of the skull and spine are not separate from either of the two tumor types. Resulting in FP in some images, our method still managed to achieve excellent segmentation execution metrics, including a mean Dice index of 82%, mean Sensitiveness of 94%, and mean Pattas value of 96%. The suggested segmentation and classification method is applicable to a variety of medical imaging situations, and our technology can assist physicians in diagnosing brain tumors. In a future study, In order to evaluate the suggested model's efficacy, we plan to develop an FCN architecture to categorize the similar MRI image dataset. Finally, we plan to look into the potential of the suggested MCNN for segmentation to be used in other areas of study, such as satellite imagery.

7 References

[1] M. Arabahmadi, R. Farahbakhsh, and J. Rezazadeh, "Deep learning for smart Healthcare—A survey on brain tumor detection from medical imaging," *Sensors*, vol. 22, no. 5, p. 1960, 2022. https://doi.org/10.3390/s22051960

[2] A. Chattopadhyay and M. Maitra, "MRI-based brain tumor image detection using CNN based deep learning method," *Neuroscience Informatics*, p. 100060, 2022. https://doi.org/10.1016/j.neuri.2022.100060

[3] M. U. Rehman, J. Ryu, I. F. Nizami, and K. T. Chong, "RAAGR2-Net: A brain tumor segmentation network using parallel processing of multiple spatial frames," *Computers in Biology and Medicine*, vol. 152, p. 106426, 2023. https://doi.org/10.1016/j.compbiomed.2022.106426

[4] K. Abdul-Hussein, M. Strelnytskyi, O. Obod, I. Svyd, and H. T. Alrikabi, "Evaluation of the interference's impact of cooperative surveillance systems signals processing for healthcare," *International Journal of Online and Biomedical Engineering (iJOE)*, vol. 18, no. 03, pp. 43–59, 2022. https://doi.org/10.3991/ijoe.v18i03.28015

[5] C.-F. Li *et al.*, "MultiR-Net: A novel joint learning network for COVID-19 segmentation and classification," *Computers in Biology and Medicine*, vol. 144, p. 105340, 2022. https://doi.org/10.1016/j.compbiomed.2022.105340

[6] N. F. Aurna, M. A. Yousuf, K. A. Taher, A. Azad, and M. A. Moni, "A classification of MRI brain tumor based on two stage feature level ensemble of deep CNN models," *Computers in Biology and Medicine*, vol. 146, p. 105539, 2022. https://doi.org/10.1016/j.compbiomed.2022.105539

[7] A. Das, S. K. Mohapatra, and M. N. Mohanty, "Design of deep ensemble classifier with fuzzy decision method for biomedical image classification," *Applied Soft Computing*, vol. 115, p. 108178, 2022. https://doi.org/10.1016/j.asoc.2021.108178

[8] B. Jena, S. Jain, G. K. Nayak, and S. Saxena, "Analysis of depth variation of U-NET architecture for brain tumor segmentation," *Multimedia Tools and Applications*, vol. 82, no. 7, pp. 10723–10743, 2023. https://doi.org/10.1007/s11042-022-13730-1

[9] Y. Chang, Z. Zheng, Y. Sun, M. Zhao, Y. Lu, and Y. Zhang, "Dpafnet: A residual dual-path attention-fusion convolutional neural network for multimodal brain tumor segmentation," *Biomedical Signal Processing and Control*, vol. 79, p. 104037, 2023. https://doi.org/10.1016/j.bspc.2022.104037

[10] S. Ali, J. Li, Y. Pei, R. Khurram, K. U. Rehman, and T. Mahmood, "A comprehensive survey on brain tumor diagnosis using deep learning and emerging hybrid techniques with multi-modal MR image," *Archives of Computational Methods in Engineering*, vol. 29, no. 7, pp. 4871–4896, 2022. https://doi.org/10.1007/s11831-022-09758-z

[11] A. Singhal, M. Phogat, D. Kumar, A. Kumar, M. Dahiya, and V. K. Shrivastava, "Study of deep learning techniques for medical image analysis: A review," *Materials Today: Proceedings*, 2022. https://doi.org/10.1016/j.matpr.2022.01.071

[12] M. Gaubert *et al.*, "Performance evaluation of automated white matter hyperintensity segmentation algorithms in a multicenter cohort on cognitive impairment and dementia," *Frontiers in Psychiatry,* vol. 13, p. 2928, 2023. https://doi.org/10.3389/fpsyt.2022.1010273

[13] T. Zhou, S. Ruan, P. Vera, and S. Canu, "A Tri-Attention fusion guided multi-modal segmentation network," *Pattern Recognition*, vol. 124, p. 108417, 2022. https://doi.org/10.1016/j.patcog.2021.108417

[14] C. Peng *et al.*, "Hypersegnas: Bridging one-shot neural architecture search with 3d medical image segmentation using hypernet," in *Proceedings of the IEEE/CVF Conference on Computer Vision and Pattern Recognition*, 2022, pp. 20741–20751. https://doi.org/10.1109/CVPR52688.2022.02008

[15] H. Yu *et al.*, "Artificial intelligence based liver portal tract region identification and quantification with transplant biopsy whole-slide images," *Computers in Biology and Medicine*, vol. 150, p. 106089, 2022. https://doi.org/10.1016/j.compbiomed.2022.106089

[16] S. Kollem *et al.*, "INCNet: Brain Tumor Detection using Inception and Optimization Techniques," in *2022 International Conference on Emerging Techniques in Computational Intelligence (ICETCI)*, 2022: IEEE, pp. 71–75. https://doi.org/10.1109/ICETCI55171.2022.9921369

[17] H. Salim and H. T. Hazim, "A novel method of invisible video watermarking based on index mapping and hybrid DWT-DCT," *International Journal of Online and Biomedical Engineering (iJOE)*, vol. 19, no. 04, pp. 155–173, 2023. https://doi.org/10.3991/ijoe.v19i04.37581

[18] N. K. Abed and I. R. ALRubeei, "Gender recognition of human from face images using multi-class support vector machine (SVM) classifiers," *International Journal of Interactive Mobile Technologies (iJIM)*, vol. 17, no. 08, 2023.

[19] Z. Lu and Z. Wang, "Researches advanced in object tracking based on deep learning," in *2nd International Conference on Artificial Intelligence, Automation, and High-Performance Computing (AIAHPC 2022)*, 2022, vol. 12348: SPIE, pp. 411–423. https://doi.org/10.1117/12.2641826

[20] J. Peng *et al.*, "Pp-liteseg: A superior real-time semantic segmentation model," *arXiv preprint arXiv:2204.02681*, 2022.

[21] J. Wolleb, R. Sandkühler, F. Bieder, P. Valmaggia, and P. C. Cattin, "Diffusion models for implicit image segmentation ensembles," in *International Conference on Medical Imaging with Deep Learning*, 2022: PMLR, pp. 1336–1348.

[22] A. Krizhevsky, I. Sutskever, and G. E. Hinton, "Imagenet classification with deep convolutional neural networks," *Communications of the ACM*, vol. 60, no. 6, pp. 84–90, 2017. https://doi.org/10.1145/3065386

[23] D. Joshi, A. Gaonkar, J. Bharambe, and A. Patil, "Deep learning approach for mammographic breast density classification and cancer risk prediction," in *2022 5th International Conference on Advances in Science and Technology (ICAST)*, 2022: IEEE, pp. 58–63. https://doi.org/10.1109/ICAST55766.2022.10039600

[24] S. H. Abbood, H. N. Abdull Hamed, M. S. Mohd Rahim, and A. H. M. Alaidi, "DR-LL Gan: Diabetic retinopathy lesions synthesis using generative adversarial network," *International Journal of Online & Biomedical Engineering*, vol. 18, no. 3, 2022. https://doi.org/10.3991/ijoe.v18i03.28005

[25] S. Primakov, E. Lavrova, Z. Salahuddin, H. C. Woodruff, and P. Lambin, "Precision-medicine-toolbox: An open-source python package for facilitation of quantitative medical imaging and radiomics analysis," *arXiv preprint arXiv:2202.13965*, 2022.

[26] S. M. Kadhem, "Iraqi sign language translator system using deep learning," *Al-Salam Journal for Engineering and Technology*, vol. 2, no. 1, pp. 109–116, 2023. https://doi.org/10.55145/ajest.2023.01.01.0013

[27] Dataset link: http://dx.doi.org/10.6084/m9.figshare.1512427

[28] H. Zhang *et al.*, "A wearable real-time character recognition system based on edge computing-enabled deep learning for air-writing," *Journal of Sensors*, vol. 2022, 2022. https://doi.org/10.1155/2022/8507706

[29] S. Dixit, A. Gaikwad, V. Vyas, M. Shindikar, and K. Kamble, "United Neurological study of disorders: Alzheimer's disease, parkinson's disease detection, anxiety detection, and stress detection using various machine learning algorithms," in *2022 International Conference on Signal and Information Processing (IConSIP)*, 2022: IEEE, pp. 1–6. https://doi.org/10.1109/ICoNSIP49665.2022.10007434

[30] N. Abiwinanda, M. Hanif, S. T. Hesaputra, A. Handayani, and T. R. Mengko, "Brain tumor classification using convolutional neural network," in *World Congress on Medical Physics and Biomedical Engineering 2018: June 3–8, 2018, Prague, Czech Republic (Vol. 1)*, 2019: Springer, pp. 183–189. https://doi.org/10.1007/978-981-10-9035-6_33

[31] E. Chatzitheodoridou, "Brain tumor grade classification in mr images using deep learning," ed, 2022.

8 Authors

Syefy Mohammed Mangj:- is a researcher at Department of medical laboratories, Technical Institute of Babylon, Al-Furat Al-Awsat Technical University. He is now a manger of center information tecnlogy at the Technical Institute of Babylon, Al-Furat Al-Awsat Technical University. His research interests is Artificial intelligence research and deep learning. (email: inb.syffi10@atu.edu.iq).

Payman Hussein Hussan:- is a researcher at Department of Computer Systems, Technical Institute of Babylon, Al-Furat Al-Awsat Technical University. Her research interests is deep learning research and biomedical analysis. (email: inb.beman10@atu.edu.iq).

Wafaa Mohammed Ridha Shakir:- [M'2005] received the Ph.D. degree in communications and electronics engineering from the University of Technology, Baghdad, Iraq, in 2011. She served as a faculty member at the technical institute of Babylon, Al-Furat Al-Awsat Technical University, Babil, Iraq since 2005. She served with the department of computer systems, Al-Furat Al-Awsat Technical University, Iraq as an Associated Professor of wireless communications engineering since 2011. She was a Research Fellow at The Pennsylvania State University, PA, USA, a Postdoctoral Fellow, at The University of Queensland, QA, Australia, and a Research Fellow at Université de Versailles Saint-Quentin-en-Yvelines, France. Her current research interests include the modeling, design, and performance analysis of wireless communication systems. (email: inb.wfa@atu.edu.iq).

Article submitted 2023-02-08. Resubmitted 2023-03-23. Final acceptance 2023-03-28. Final version published as submitted by the authors.